Tribology International 77 (2014) 78–85

Contents lists available at ScienceDirect

Tribology International

journal homepage: www.elsevier.com/locate/triboint

Modeling the edge contact effect of finite contact lines on subsurface stresses

Morteza Najjari, Raynald Guilbault *

Department of Mechanical Engineering, École de technologie supérieure, 1100 Notre-Dame Street West, Québec, Montréal, Canada H3C 1K3

ARTICLE INFO

Article history:
Received 24 January 2014
Received in revised form
10 April 2014
Accepted 22 April 2014
Available online 30 April 2014

Keywords:
Subsurface stresses
Finite line contact
Edge influence
Quarter-space

ABSTRACT

Finite contact line conditions lead to subsurface stress distributions determined by the free boundaries. Combined with a correction procedure, Semi-Analytical Methods (SAMs) accurately include the free boundary effects, and represent a rapid alternative to the Finite Element Method (FEM) for contact pressure calculation. This paper extends the free boundary correction procedure to the evaluation of surface and subsurface stresses from SAMs. The investigation integrates a validation based on a two-level factorial comparison confronting the stress distributions established with the developed procedure to results obtained from FEM models. The comparison examines three dimensionless factors, and shows that the stress distributions are evaluated with a high level of precision. The model also offers evaluation more than 125 times faster than FEM simulations.

1. Introduction

Non-conformal contact interfaces undergo severe stress fields [1]. Finite contact line conditions existing in applications such as gears or cams may present additional stress concentrations close to the associate free boundaries and resulting edges [2]. Under Hertzian conditions, the maximum shear defining the contact critical area appears at a short distance beneath the surface. The presence of free boundaries, asperity contact or sliding (non-Hertzian contact) may affect the location of the maximum value of the stresses [3,4]. However, under any conditions, the surface and subsurface stress distributions are controlling factors of the contact fatigue life. Therefore, accurate rolling contact fatigue life prediction requires precise descriptions of stress fields near discontinuity zones [5–11].

Since contact pressure distribution evaluation is essential for obtaining the surface and subsurface stress fields, under non-Hertzian contact conditions, numerical modeling becomes inevitable. The Finite Element Method (FEM) often appears as the easiest approach. Nevertheless, obtaining the necessary precision requires very fine FEM meshes, normally resulting in prohibitive calculation times. Alternatively, Semi-Analytical Methods (SAMs) based on the Boussinesq–Cerruti solution for point tractions acting on elastic half-space represent an efficient way to deal with the pressure distribution problem. The half-space assumption also offers closed-form expressions for stress calculation [12,13]. However, this approach is obviously unable to account for finite contact interfaces, and, consequently, leads to non-realistic values close to or at the contact extremities. Hence, when applied to such conditions, SAMs need to be corrected. For the pressure calculation, Hetényi [14,15] proposed the application of virtual mirrored pressures for shear stress elimination and an iterative treatment for normal stress correction. Recently, Guilbault [16] introduced a correction factor (Eq. (1)) which multiplies the mirrored pressures to simultaneously correct the shear and normal stress influence on the surface displacements. Compared to the complete Hetényi process, because it eliminates the iterative treatment, this last procedure drastically reduces the calculation times. Once the corrected pressure distribution is established, the surface and subsurface stresses may be evaluated with the closed-form expressions available in the literature [17–23]. However, to the author's knowledge, the literature provides no particular adaptation procedure for those expressions, and therefore, the underlying half-space assumption once again leads to unsound stress evaluations close to the body limits

$$\psi = 1.29 - \frac{1}{1-\nu}(0.08 - 0.5\nu) \tag{1}$$

This paper introduces a simple complementary correction procedure for surface and subsurface stress evaluation in real delimited bodies. The study includes a validation section in which a two-level factorial comparison incorporating three dimensionless factors confronts the stress distributions established with the developed procedure to results obtained from FEM models.

* Corresponding author. Tel.: +1 514 396 8862; fax: +1 514 396 8530.
E-mail addresses: morteza.najjari.1@ens.etsmtl.ca (M. Najjari), raynald.guilbault@etsmtl.ca (R. Guilbault).

http://dx.doi.org/10.1016/j.triboint.2014.04.024
0301-679X/

Nomenclature

γ	Stress transition factor
ν	Poisson ratio
ψ	Guilbault's correction factor
ρ	Spatial radius
τ_{max}	Maximum shear stress
σ_{ij}	Stress tensor
a	Half-length of a cell
b	Half-width of a cell
C	Half-width of Hertzian contact
E	Young modulus
E^*	Contact modulus
$f_{ij,kl}$	Flexibility matrix
L_1, L_2	Length of bodies 1 and 2
L_r	Dimensionless contact length ratio
P', P''	Mirrored pressures
P_{kl}	Cell constant pressure
R	Equivalent roller radius
S_l	Dimensionless contact slenderness
u_{ij}	Deflection of a cell
w	Load
W	Dimensionless load factor
x_g, y_g, z_g	Global coordinate system
x, y, z	Local coordinate system
$\bar{x}$, $\bar{y}$, $\bar{z}$	Relative position

2. Contact of two elastic bodies

2.1. Pressure distribution

The general dry contact problem resolution procedure is well described and validated in Ref. [16]. In the present paper, the contact pressure distributions are obtained from the same algorithm. Fig. 1 illustrates the procedure when applied on two of the free boundaries (F_{b1} and F_{b2}) of a roller/rectangular body contact problem; the solution domain is divided into constant pressure cells of lengths $2a$ and $2b$ in the x and y directions, and the flexibility matrix written for the resulting mesh. Eq. 2 gives the flexibility coefficients for a cell ij of the surface, when pressure (P) is applied on a cell kl. In order to account for the body limits, the pressure cells are mirrored with respect to the free boundaries (P' for F_{b1} and P'' for F_{b2}), and their influence integrated into the flexibility matrix. The first correction eliminates the free boundary artificial shear stress. To remove the remaining normal stress influence, each mirror cell contribution is multiplied by Guilbault's factor (ψ, Eq. (1)) prior to its integration into the flexibility matrix. This last operation completely releases the boundaries. Eq. 3 establishes the relation between the pressure distribution and the surface displacement at position (i, j)

$$f_{ij,kl}=\left\{\begin{array}{l}(x_{ik}+a)\ln\left[\dfrac{(y_{jl}+b)+\sqrt{(x_{ik}+a)^2+(y_{jl}+b)^2}}{(y_{jl}-b)+\sqrt{(x_{ik}+a)^2+(y_{jl}-b)^2}}\right]+\\ (x_{ik}-a)\ln\left[\dfrac{(y_{jl}-b)+\sqrt{(x_{ik}-a)^2+(y_{jl}-b)^2}}{(y_{jl}+b)+\sqrt{(x_{ik}-a)^2+(y_{jl}+b)^2}}\right]+\\ (y_{jl}+b)\ln\left[\dfrac{(x_{ik}+a)+\sqrt{(x_{ik}+a)^2+(y_{jl}+b)^2}}{(x_{ik}-a)+\sqrt{(x_{ik}-a)^2+(y_{jl}+b)^2}}\right]+\\ (y_{jl}-b)\ln\left[\dfrac{(x_{ik}-a)+\sqrt{(x_{ik}-a)^2+(y_{jl}-b)^2}}{(x_{ik}+a)+\sqrt{(x_{ik}+a)^2+(y_{jl}-b)^2}}\right]\end{array}\right\} \quad (2)$$

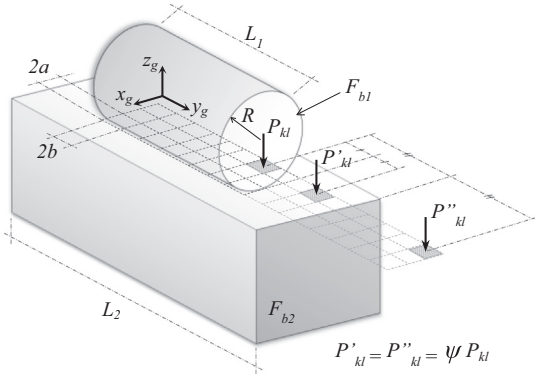

Fig. 1. Roller and rectangular body contact.

$$u_{ij}=\left(\frac{1-\nu^2}{\pi E}\right)\sum_{k=1}^{n_x}\sum_{l=1}^{n_y}f_{ij,kl}p_{kl} \quad (3)$$

2.2. Stress distribution

The expressions for the surface and subsurface stress produced by a contact pressure acting on a rectangular patch on the surface of an elastic half-space were first presented by Love [19]. Based on these expressions, the stress tensor at any point $p\,(x_p, y_p, z_p)$ of the half-space resulting from pressures distributed over constant pressure cells kl is written as presented by Eqs. (4)–(10) [23]:

$$\sigma_{mn|\bar{x},\bar{y},\bar{z}}=\left(\frac{1}{2\pi}\right)\sum_{k=1}^{n_x}\sum_{l=1}^{n_y}p_{kl}\left(\begin{array}{l}A_{mn}(\bar{x}+a,\bar{y}+b,\bar{z})+A_{mn}(\bar{x}-a,\bar{y}-b,\bar{z})\\ -A_{mn}(\bar{x}-a,\bar{y}+b,\bar{z})-A_{mn}(\bar{x}+a,\bar{y}-b,\bar{z})\end{array}\right) \quad (4)$$

with

$$A_{xx}(x,y,z)=2\nu\left[\tan^{-1}\left(\frac{xz}{y\rho}\right)-\tan^{-1}\left(\frac{x}{y}\right)\right]-\tan^{-1}\left(\frac{y}{x}\right)+\tan^{-1}\left(\frac{yz}{x\rho}\right)+\frac{xyz}{\rho(x^2+z^2)} \quad (5)$$

$$A_{yy}(x,y,z)=2\nu\left[\tan^{-1}\left(\frac{yz}{x\rho}\right)-\tan^{-1}\left(\frac{y}{x}\right)\right]-\tan^{-1}\left(\frac{x}{y}\right)+\tan^{-1}\left(\frac{xz}{y\rho}\right)+\frac{xyz}{\rho(y^2+z^2)} \quad (6)$$

$$A_{zz}(x,y,z)=-\tan^{-1}\left(\frac{y}{x}\right)-\tan^{-1}\left(\frac{x}{y}\right)+\tan^{-1}\left(\frac{yz}{x\rho}\right)+\tan^{-1}\left(\frac{xz}{y\rho}\right)-\frac{xyz}{\rho(x^2+z^2)}-\frac{xyz}{\rho(y^2+z^2)} \quad (7)$$

$$A_{xy}(x,y,z)=(2\nu-1)\ln(\rho+z)-\frac{z}{\rho} \quad (8)$$

$$A_{xz}(x,y,z)=\frac{yz^2}{\rho(x^2+z^2)} \quad (9)$$

$$A_{yz}(x,y,z)=\frac{xz^2}{\rho(y^2+z^2)} \quad (10)$$

where $\rho=\sqrt{x^2+y^2+z^2}$, $\bar{x}=x_k-x_p$, $\bar{y}=x_k-y_p$ and $\bar{z}=z_p \quad (z_p\geq 0)$.

Fig. 2 shows the 3D stress state obtained for a quarter-space defined by one free boundary, when treated with the previous equation. As before with the pressure calculation, the half-space assumption generates artificial normal and shear stresses on the free surface. In reality, σ_{yy}, σ_{yz} and σ_{yx} are null at the free boundary. Therefore, once the pressure distribution is evaluated, the stress distribution computation also demands a free boundary stress elimination.